Int. J. Heat Mass Transfer. Vol. 33, No. 7, pp. 1397–1415, 1990
Printed in Great Britain

0017-9310/90 $3.00 + 0.00
Pergamon Press plc

Hydrodynamics and heat transfer in a vertical cylinder exposed to periodically varying centrifugal forces (accelerated crucible-rotation technique)

A. G. KIRDYASHKIN and V. E. DISTANOV
Institute of Geology and Geophysics, Siberian Branch of the U.S.S.R. Academy of Sciences, Novosibirsk, U.S.S.R.

(*Received* 5 *April* 1988)

Abstract—Investigations are made of the thermal and hydrodynamic structure of liquid flow in a vertical cylinder exposed to the simultaneous effect of thermal gravitational and periodically varying centrifugal forces. The latter were produced by periodic variation of the rotational speed of the cylinder, the axis of which coincided with that of rotation. A vortex flow is found at the bottom of the cylinder, the direction of which depends on the rotational speed of the latter. The hydrodynamics and heat transfer of the liquid stably stratified over the height and exposed to periodically varying centrifugal forces are investigated. It is shown that there are periodic changes of temperature throughout the entire liquid layer; the values of temperature and velocity and their variations at different liquid layer heights are found. The effect of periodically varying forces on the quality of a growing crystal is analysed. The paper might be of interest for thermal physicists and specialists dealing with the growth of monocrystals.

INTRODUCTION

GROWTH OF crystals in a crucible without forced mixing in a melt occurs in the presence of free convection generated by temperature and concentration gradients in the melt. In most cases free convection does not produce considerable melt stirring and influences the process of crystallization only in the case of small growth rates [1]. Forced convection enhances the convective mass transfer rate. It can be induced either by mechanical agitation or by melt exposure to physical fields (e.g. ultrasonic and electromagnetic).

Melt stirring by means of the field of body forces seems to be complicated enough as it requires the creation of special technological equipment. Moreover, the field-induced stirring of the melt may give rise to factors which adversely affect the quality of monocrystals being grown. For instance, crystallization with melt stirring by ultrasound is accompanied by the formation of numerous crystallization centres in the melt and also by the 'destruction of tiny single crystals already grown' [2]. The fragments of these monocrystals act as new crystallization centres (the process proceeds within a wide range of frequencies—from 2×10^2 to 9×10^6 Hz—and at high enough ultrasound levels). In addition, container vibrations may be accompanied by the formation of 'spurious' nuclei at the walls and bottom of the container and this results in ingot inhomogeneity [3]. The ultrasound field influences diffusion fluxes and heat transfer, which are basic parameters of crystallization [1]. The mixing of a melt by an electromagnetic field can be applied only for electrically conducting liquids, and this restricts its field of application.

Mechanical stirring of a melt is widely employed in the growth of monocrystals. Mechanical mixers commonly used for stirring when growing monocrystals from aqueous solutions are not suitable for reactive decomposable melts, such as proustite (Ag_3AsS_3). In these cases it is expedient that the stirring of the melt be accomplished by the rotation of a container about its longitudinal axis. In the growing of monocrystals, the container is rotated at any inclination to the horizon, specifically in vertical and horizontal crystallization.

It was shown in the works of Sheel and Shultz-Du Bois [4, 5] that uniform rotation of the crucible does not lead to complete mixing of the melt. Moreover, it is even less effective than stirring by free convection. All the same, some authors recommended the use of uniform rotation of the crucible to decrease temperature gradients in furnaces with the temperature asymmetry [1, 6].

The accelerated crucible-rotation technique (ACRT) for growing monocrystals was used for the first time by Sheel and Shultz-Du Bois. They formulated the basic conditions for obtaining qualitative monocrystals from solution–melt and suggested the use of periodic decreases and increases in the rotational speed of a crucible for stirring of melts [4, 7].

To obtain large monocrystals by the solution–melt method it is necessary: (i) to control the nucleation; (ii) to provide a high enough flow of melt on the interface; (iii) to guard against constitutional supercooling; and (iv) to prevent dendritic growth after nucleation. These requirements are met by applying the method of modulated rotation of a crucible with local cooling of its bottom.

NOMENCLATURE

a	thermal diffusivity
d	diameter of bulb
g	acceleration of gravity
H	height of the working layer of liquid (from heater to temperature-controlled substrate)
K	coefficient of incident radiation absorption for ordinary beam
l	length of bulb
n	number of revolutions per minute
Pr	Prandtl number, ν/a
Q	liquid discharge
r	radius of bulb
Re	Reynolds number, $\omega r^2/\nu$
T	temperature
Ta	Taylor number, $(\omega_{max}^2-\omega_0^2)r^4/\nu^2$ where $\omega_0=(\omega_{max}+\omega_{min})/2$
T_{boil}	boiling temperature
u	horizontal velocity
v	vertical velocity
x	horizontal coordinate
y	vertical coordinate.

Greek symbols

β	coefficient of thermal expansion of liquid
δ	dynamic boundary layer thickness
θ	boundary layer temperature near cylinder generatrix, $T-T_0(y)$
θ_1	$T_1-T(y)$, where T_1 is the temperature of cylinder generatrix
λ	incident radiation wavelength
ν	kinematic viscosity
τ	time
ϕ/ϕ_0	optical resolution
ω	angular velocity of the rotation bulb.

Subscripts

c	temperature-controlled bottom of bulk
max	maximum value
min	minimum value
rel	relative number
0	parameters of flow core
1	ascending flow
2	descending flow.

Superscript

¯	mean quantity.

In the growing of crystals from both solutions and melts, the stirring decreases the diffusion layer thickness at the crystallization front. When growing crystals by the solution–melt method with periodic variation of the rotational speed of a crucible, the diffusion layer thickness decreased by factors of 1.4 [8] and 2 [9] for $Y_3Fe_5O_{12}$ and by an order of magnitude [7] for $GdAlO_3$.

Experience in the growing of crystals from aqueous solutions shows that superfluous agitation of the solution does not favour the growing of high-quality monocrystals [10]. Therefore, instead of an instantaneous increase in the crucible rotation speed from zero to the maximum, Sheel and Shultz-Du Bois suggested the use of smooth acceleration and deceleration of the crucible rotation [4]. They found in model tests that the melt streams in the vicinity of the growing face of a crystal look like spirals. Three types of cycles of rotational speed variation were used: a sawtooth cycle with rotation in one direction, a sawtooth cycle with rotation in both directions and a truncated sawtooth time cycle with rotation in both directions [4, 11]. The maximum rotational speed of the crucible depends on its diameter and on the thermophysical properties of the melt. For example, for growing boron monophosphide (BP) crystals, Chu *et al.* [11] used a maximum speed of 120 r.p.m., with acceleration $\pm 0.4\ \pi$ rad s^{-2}. The period varied from several seconds to one minute. Good results were obtained even in long and thin crucibles (13 cm long, 15 mm i.d., 20 mm o.d.), where the effect of accelerated rotation is not so pronounced as in large-diameter bulbs (40–50 mm). The maximum rotational speed in growing monocrystals of $Y_3Fe_5O_{12}$ [12] was 50 r.p.m., with the diameter of the crucible about 70 mm.

The ACR technique allows one to substantially increase the size and quality of crystals grown from solution–melt. Sheel indicated the possibility of the use of this technique in the Czochralski method [7]. The technique was also applied to zonal purification of substances. At the Institute of Physical Chemistry (Amsterdam, Holland) special apparatus was designed [13] which decreased the diffusion layer thickness by reversible high-speed rotation. The maximum speed attained was 125 r.p.m., and the direction of rotation changed twice a second. The time required for a reversible change in the speed of rotation from 125 r.p.m. in one direction to 125 r.p.m. in the other direction amounted to about 0.25 s. With this technique Bollen *et al.* [13] managed to obtain effective coefficients of impurity distribution which were close to those predicted theoretically. For example, in the biphenyl–phenanthrene system, which forms solid solutions, the theoretical coefficient of distribution is equal to 0.27. The ACR technique gave a coefficient approaching 0.30. Such a small difference allows one to find the distribution coefficients for unknown substances of mixtures from the results of zone melting.

Earlier investigations [4, 5] showed that the ACR

technique is very effective for melt mixing. It can also be used efficiently for growing monocrystals from melts [7]. It allows one to substantially increase the quality and size of crystals grown due to a more intensive stirring of the melt and smaller diffusion layer thickness at the crystallization front.

The ACR technique is also used for growing monocrystals from melts by Stockbarger's method. It allowed one for the first time to obtain monocrystals of proustite (Ag_3AsS_3) of large diameter and with a high optical quality [14–16]. The technique was also employed successfully in Bridgman's method for growing high-quality monocrystals of the incongruently fusing compound Rb_2MnCl_2 from non-stoichiometric melts [17]. The technique made it possible to increase the growth rate of monocrystals (three times for Ag_3AsS_3 and four times for Rb_2MnCl_4) without impairing their optical quality and increasing inclusions.

The foregoing served as the basis for initiating investigations into the hydrodynamics and heat transfer of melts in model experiments and their influence on the process of crystallization.

The problems of liquid flow around a rotating disk and about a fixed disk in a rotating liquid have been well studied [18]. The present understanding of the hydrodynamic structure of liquid near the rigid end face surface of a cylinder with a periodically varying speed of rotation is inadequate and has been studied only qualitatively [5].

Still more complex flow should be expected in the case of periodic variation of centrifugal forces when the plane bottom of a vertical cylinder is cooled and when the conditions for stable stratification and a horizontal temperature gradient develop. It is these very conditions that originate in the process of crystal growth from a melt by the ACR technique.

The present paper considers the results of theoretical and experimental investigations of the hydrodynamics and heat transfer in a vertical cylinder in the absence of rotation and in the case of periodically varying centrifugal forces, when the liquid is heated from above and is cooled from below and along the cylinder generatrices. Analysis of the effect exerted by the thermal and hydrodynamic structure of melt on the quality of a crystal is carried out.

A FIXED VERTICALLY ORIENTATED CYLINDRICAL GLASS BULB

The growing of monocrystals from a melt in a vertically orientated bulb (Stockbarger's method) is widely used at present for obtaining optical crystals of decomposable compounds, such as complex chalcogenides, which require complete encapsulation and absence of contact with the surroundings. In this case the transfer processes in bulbs, differently orientated with respect to gravitational acceleration, are governed by thermal–gravitational and concentrational–gravitational convection in melts and also by diffusion. The concentration fields depend substantially on temperature gradients in the bulb on their orientation with respect to the gravitational acceleration.

For the vertical orientation of the cylindrical bulb axis (Stockbarger's method) the conditions for the growth of crystals are created by a cylindrical heat exchanger separated by a diaphragm, i.e. there is an elevated temperature in the upper part of the melt and a reduced temperature at the bottom, in the region of the crystallization front. It is of interest to find the temperature and velocity distributions in a stationary bulb heated from above and cooled in the region of the growing face of a crystal (Fig. 1). In this case, heat is mainly removed from the side walls of the bulb when the heated zone is located at a great distance (as compared with the cylinder radius) from the bulb end face. A free convection boundary layer and a descending flow are formed on the inner surface of the bulb, and an ascending flow is formed in the bulb 'core'. In this 'core' region (i.e. outside the horizontal boundary layer near the free surface and vertical boundary layers at the cylinder generatrices), the viscous forces are vanishingly small for a large-scale flow and the horizontal temperature gradient under steady-state conditions is also small [19]. Arbitrarily small horizontal gradients give rise to horizontal flows which equilibrate the temperature over 'r', i.e. in the flow core T_0 depends only on $y = T_0(y)$. With the assumption that vertical flows are possible which depend on y, $v(y)$ and $T_0 = T_0(y)$, the continuity equation gives

$$u = u(y)x + c$$

where u is the horizontal velocity component. Under the assumption $v = v(y)$, steady-state horizontal flows should exist which can be induced by horizontal temperature gradients in the flow core provided there is cooling of the side walls, i.e. T_0 also depends on x. This means that the assumption about the iso-

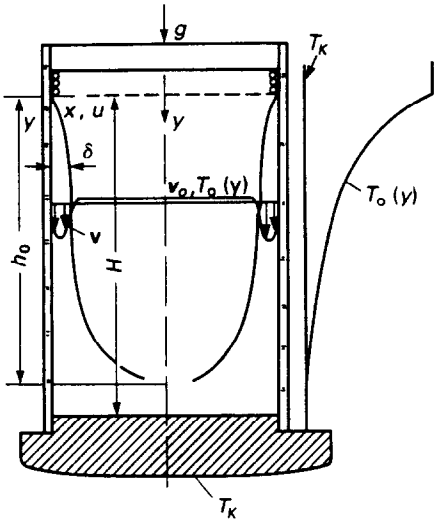

FIG. 1. Scheme of thermal gravitational flows in a fixed bulb.

thermicity over the horizontal and the existence of stable stratification ($T_0(y)$) require the fulfillment of the condition $v_0 = \text{const.}$, i.e. that v_0 also be independent of y.

The flow core is described by the following equation:

$$v_0 \frac{\partial T_0}{\partial y} = a \frac{\partial^2 T_0}{\partial y^2}. \tag{1}$$

Under the boundary conditions $y \to \infty$, $\partial T/\partial y = 0$, $y = 0$, and $T = T_{max}$, the solution has the form

$$T_0 = T_{max} \cdot e^{-(v_0/a)y} \tag{2}$$

where the temperature is calculated from $T_0(\infty)$, a is the thermal diffusivity and $-v_0$ is the vertical velocity component directed upwards. Temperature measurements along the height of the stationary bulb heated from above and cooled from the sides and bottom confirm relation (2) (Fig. 2).

Thus, for a stationary vertical bulb the typical temperature distribution in the flow core is that given by equation (2), $v_0 = \text{const}$. The typical relation for the boundary layer on the wall is

$$\int_0^{\delta} v(y)\,dx = \text{const}. \tag{3}$$

Now, the development of the free convective boundary layer over the cylinder generatrices will be considered (Fig. 1). It is assumed that $\delta \ll r_0$.

Under the Boussinesq approximation, the equations of thermal gravitational convection have the form [19]:

$$v\frac{\partial v}{\partial y} + u\frac{\partial v}{\partial x} = \nu\frac{\partial^2 v}{\partial x^2} - \beta g(T - T_0(y)) \tag{4}$$

$$v\frac{\partial T}{\partial y} + u\frac{\partial T}{\partial x} = a\frac{\partial^2 T}{\partial x^2} \tag{5}$$

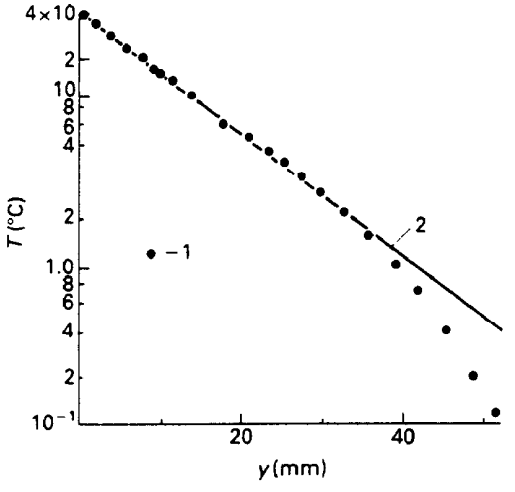

FIG. 2. Temperature distribution in the core of the liquid layer in a bulb ($H = 85$ mm). 1. Experimental values. 2. Equation (2).

$$\frac{\partial v}{\partial y} + \frac{\partial u}{\partial x} = 0. \tag{6}$$

The boundary conditions are

$$\text{at} \quad x = 0, \quad v = 0, \quad u = 0, \quad T = T_1 \tag{7}$$

or

$$(\partial T/\partial x)_{x=0} = T_1' \quad \text{at} \quad x = \infty, \quad v = 0$$
$$\partial T/\partial x = 0, \quad T = 0.$$

Here ν is the kinematic viscosity, β is the coefficient of volumetric expansion and g is the gravitational acceleration.

Let the solution be represented in the form

$$T = T_0(y) + \theta(x, y). \tag{8}$$

Then, equation (5) can be written as

$$v\frac{\partial T_0}{\partial y} + v\frac{\partial \theta}{\partial y} + u\frac{\partial \theta}{\partial x} = a\frac{\partial^2 \theta}{\partial x^2}. \tag{9}$$

In the case considered $v\theta \ll vT_0$ and, consequently, the second term in equation (9) is much smaller than the first term. Since

$$\int_0^{\delta} v\,dx = \text{const}.$$

therefore $u \ll v$ (δ is the dynamic boundary layer thickness). Thus equation (9) can be represented as

$$v\frac{\partial T_0}{\partial y} = a\frac{\partial^2 \theta}{\partial x^2}. \tag{10}$$

In equation (4) the inertia term $u(\partial v/\partial x)$ will be neglected (because of the smallness of u) as well as the term $v(\partial v/\partial y)$, which is valid at high Prandtl numbers, $Pr = \nu/a > 1$:

$$\nu\frac{\partial^2 v}{\partial x^2} = \beta g\theta. \tag{11}$$

The boundary conditions (7) will be written as

$$x = 0, \quad v = 0, \quad \theta = \theta_1 \ (\text{or } \partial\theta/\partial x = \theta_1');$$
$$x = \infty, \quad v = 0, \quad \theta = 0. \tag{12}$$

Differentiating equation (11) twice with respect to x and substituting $\partial^2\theta/\partial x^2$ into equation (10) yields

$$\frac{\partial^4 v}{\partial x^4} + v\frac{\beta g}{a\nu}\left(-\frac{\partial T_0}{\partial y}\right) = 0. \tag{13}$$

Let

$$4m^4 = \frac{\beta g}{a\nu}\left(-\frac{\partial T_0}{\partial y}\right); \tag{14}$$

since $\partial T_0/\partial y < 0$, then $4m^4 > 0$.

The solution to the equation

$$(D^4 + 4m^4)v = 0 \quad (D = d/dx)$$

at $v(0) = 0$ and $v(\infty)$ has the following general form:

$$v = c \cdot \sin mx \cdot e^{-mx}. \tag{15}$$

Differentiating equation (14) twice with respect to x and substituting the resulting expression $\partial^2 v/\partial x^2$ into equation (11) gives

$$-m^2 2c \cdot e^{-mx} \cos mx = \frac{\beta g \theta}{\nu}. \quad (16)$$

With regard to the fact that $\theta = \theta_1$ at $x = 0$, equation (15) gives

$$c = \frac{\beta g \theta_1}{2\nu m^2}.$$

When the liquid is cooled, $\theta_1 < \theta$, as follows from equation (8). The solution for v has the form

$$v = \frac{\beta g \theta_1}{2\nu m^2} \sin mx \cdot e^{-mx}. \quad (17)$$

With $\partial^2 v/\partial x^2$ substituted into equation (11), equation (16) yields

$$\theta = \theta_1 \cdot e^{-mx} \cdot \cos mx. \quad (18)$$

Since $\delta \ll r_0$, then

$$v_0 \pi r_0^2 = 2\pi r_0 \int_0^x v \, dx.$$

Then, substituting equation (16) into the latter relation and integrating it, we obtain

$$v_0 = \frac{\beta g \theta_1}{2\nu m^3 r_0}. \quad (19)$$

With the use of the second representation of boundary conditions at $x = 0$ for $\partial\theta/\partial x = \theta_1'$, the solution of equations (10) and (11) gives

$$v = \frac{\beta g \theta_1'}{2\nu m^3} e^{-mx} \sin mx \quad (20)$$

$$\theta = -\frac{\theta_1'}{m} e^{-mx} \cos mx \quad (21)$$

$$v_0 = -\frac{\beta g \theta_1'}{2\nu m^4 r_0}. \quad (22)$$

The liquid temperature measurements were carried out in a stationary vertically orientated bulb 29 mm in diameter and 125 mm in height. The bulb had a copper bottom which was kept at a controlled temperature, $T_c = 24.5$°C. The bulb encased a fluoroplastic cylinder 28 mm in diameter and 40 mm long which had a 4 mm deep slit over the diameter and along the entire length for inserting a Γ-shaped probe. A 0.05 mm diameter nichrome–constantan thermocouple was displaced, with the aid of a transverse mechanism, along the height and radius of the cylinder in one plane passing through the bulb axis. The radial displacement of the probe was controlled by a B-630 cathetometer positioned on the transversing table and with the aid of a displacement indicator accurate to 0.002 mm; the reference point was taken to be any point on the thermocouple transverse mechanism which rested on a rigid stationary rack. The vertical displacement was controlled by a B-630 cathetometer to 0.01 mm. The needle-type thermocouple probe was brought into close contact with the bulb wall. The contact was confirmed by the appearance of constant e.m.f. The coordinate of the wall was determined from the plot of the measured e.m.f. of the thermocouple vs r, i.e. from the intersection of the straight line for the constant e.m.f. of the thermocouple with the temperature profile in the wall region. The e.m.f.s of the thermocouple were measured by a P-3003 comparator accurate to 1 μm. The cold junction of the thermocouple was positioned on the copper bottom of the bulb. A circular heater was attached around the bulb perimeter in the upper part of the liquid layer. It was a 0.5 mm thick fluoroplastic ring with a doubly wound wire 0.2 mm in diameter fixed on the fluoroplastic cylinder in the bulb at a distance of about 12 mm from its bottom. The heater was fed by a stabilized constant voltage source.

To decrease the disturbances, the upper boundary of the working liquid (96% ethyl alcohol) was brought into contact with the lower end face of the fluoroplastic cylinder. The measurements were taken in steady-state conditions every 3–4 h after the set-up was switched on.

The results of temperature measurements along the height of the ethyl alcohol layer ($H = 85$ mm) at its centre are presented in Fig. 2. Over the greater portion of the liquid layer below the heater the temperature varies according to equation (2). The reference point along the coordinate (y) is taken to be the position of the heater end face. The temperature of the bulb copper bottom is taken as the reference temperature. It is seen from Fig. 2 that in the core of the bulb $T_0 = 40\, e^{-89y}$ (where y is in m) for y lying within the range $0 \leqslant y \leqslant 35$ mm. According to equation (2), at $a = 0.842 \times 10^{-7}$ m^2 s^{-1} and $T_{av} = 40$°C, the quantity $v_0 = 7.5 \times 10^{-6}$ m s^{-1}. On obtaining v_0 from equations (14) and (19), it is possible to determine θ_1. The velocity and temperature profiles are calculated from equations (14), (17) and (18). The calculated velocity and temperature profiles in the boundary layer at the bulb wall for different values of y are presented in Figs. 3(a)–(c); a comparison is also made between the measured temperature differences $\theta - \theta_1$ (dots) and those calculated from equations (14), (17) and (18) (curve 2). There is a good agreement between theory and experiment. Deviations appear when $y < 2.5$ because of the penetration of thermal and hydrodynamic disturbances from the unstably stratified region of the layer under the heater. The temperatures measured outside the boundary layer (in the flow core) at $y = \text{const.}$ are presented in Figs. 4(a)–(c). The measurements were made under the same conditions as in Fig. 2. With approach to the bulb axis the temperature of the flow core slightly increases. Thus, for the boundary conditions considered the approximations adopted for the theoretical analysis of hydrodynamics and heat transfer in a stationary vertical bulb are quite reasonable.

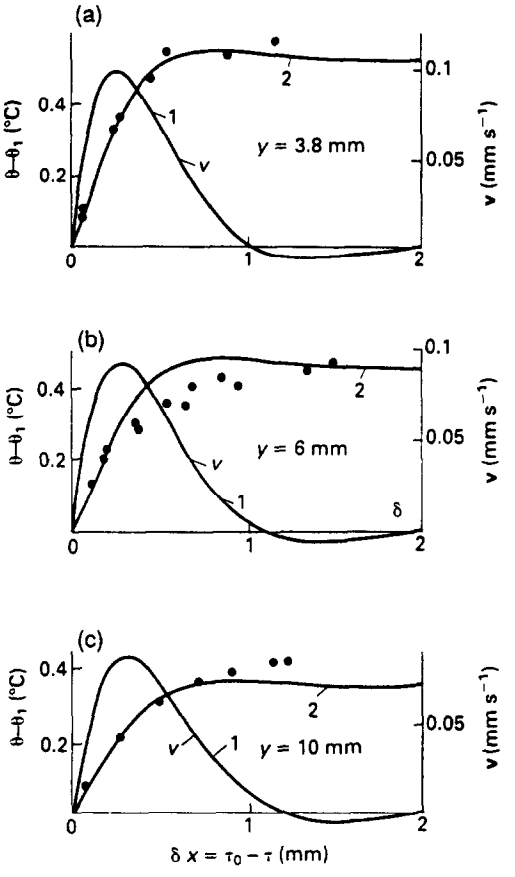

FIG. 3. Velocity (1) and temperature (2) profiles in the boundary layer at the bulb wall. 1, According to equations (14) and (17). 2, According to equations (14) and (18). 3, Experimental values of temperature $(\theta-\theta_1)$; (a) $y = 3.8$ mm; (b) $y = 6$ mm; (c) $y = 10$ mm.

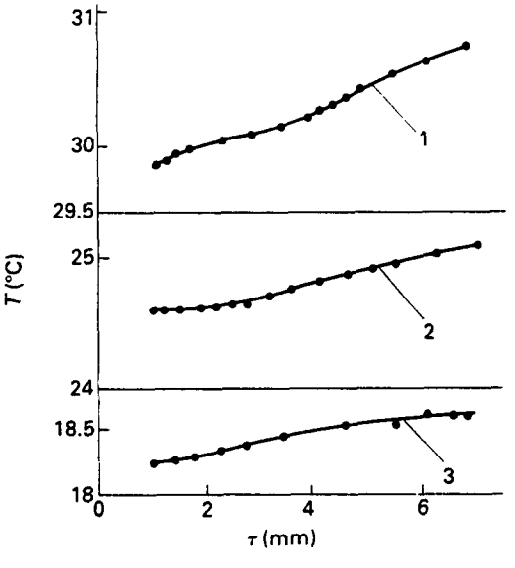

FIG. 4. Temperature in the flow core at $y = \text{const.}$, $H = 85$ mm. 1, $y = 2.89$ mm. 2, 5.02 mm. 3, 9.82 mm.

PERIODIC VARIATION OF THE ROTATIONAL SPEED OF THE CYLINDRICAL BULB

Depending on the height of the melt in the bulb, the temperature field near the growing face of a crystal varies and can be non-uniform, thus entailing the non-uniform growth of the crystal and the appearance of structural and optical non-uniformities.

Therefore, it was suggested earlier [14, 16, 20] that for growing monocrystals by the Stockbarger method the melt in the bulb should be stirred by periodically varying the number of revolutions by the given modulation law. Let this technique be called the technique of modulated rotation.

Experimental investigations of the hydrodynamic and thermal structures of the melt in the bulb were made on a set-up shown in Fig. 5(a). The set-up made it possible:

(1) to vary the angular rotational speed of the table with the bulb according to the trapezoidal law with any relationship between the rate of increase and

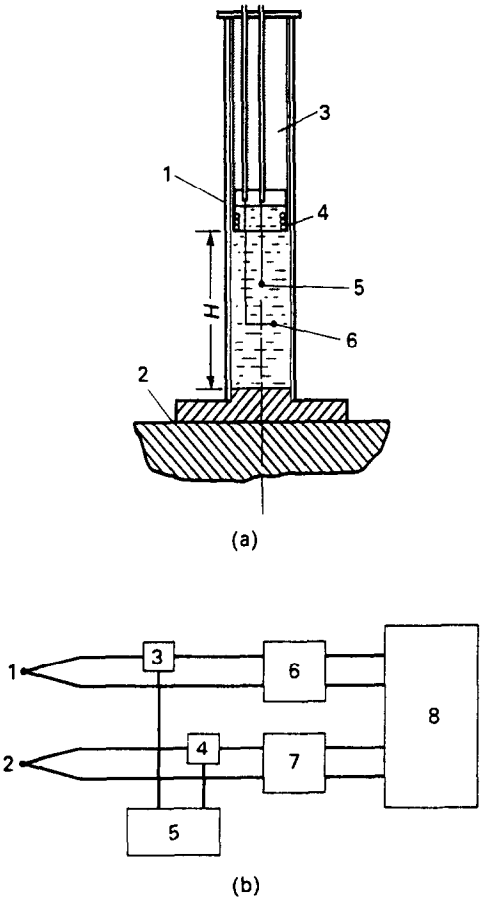

FIG. 5. (a) Scheme of an experimental bulb. (b) Block diagram of the measurement of instantaneous temperature values in the layer. 1, 2, Thermocouples. 3, 4, Compensational potentiometers. 5, Voltage comparator. 6, 7, Constant current amplifiers. 8, Two-channel self-recording potentiometer.

decrease in the angular speed ω and the time intervals $\tau_{max} \leqslant 5$ min ($n_{max} = 300$ r.p.m.) for $\omega = \text{const.}$; there was provision for reversible rotation;

(2) to measure temperatures simultaneously using eight thermocouples with the aid of sliding contacts; to measure e.m.f. within ∓ 2 μV; power from two generators was delivered to the table with the bulb;

(3) to control the temperature of substrate ('crystal') by supplying temperature-controlled water;

(4) to take still photographs of the liquid velocity field in the bulb;

(5) to orientate the axis of rotation of the table with the bulb from the vertical to horizontal position.

EXPERIMENTAL PROCEDURE

A transparent cylindrical bulb (Fig. 5(a)) made of glass (1) with an inner diameter of 29 mm and length 125 mm was positioned co-axially with the rotational axis of the table (2); the metallic bottom of the bulb which modelled the plane front of crystallization contacted with the temperature-controlled copper base ($T_c = 24.5$°C). The bulb encased a 28 mm diameter and 95 mm long fluoroplastic cylinder (3). The lower part of this cylinder was hollow and had an inner diameter of 28 mm. On the cylinder generatrix a heat exchanger (4) was located which was made of a doubly wound 8 mm high spiral of wire 0.2 mm in diameter. The upper turn of the spiral was 10 mm below the free surface of the liquid to avoid the introduction of additional hydrodynamic disturbances on acceleration or deceleration of rotation and to ensure an easy variation of the liquid height by means of raising or lowering the fluoroplastic cylinder. The temperature in the volume of the liquid was measured by two nichrome–constantan thermocouples made of 0.005 mm diameter wires. One thermocouple probe was positioned at the axis of the fluoroplastic cylinder and measured the temperature along the axis of the liquid layer (5). The Γ-shaped thermocouple (6) was imbedded in the recess drilled in the fluoroplastic cylinder; it could be moved in the vertical and radial directions. The coordinates of the thermocouples were measured by a B-630 cathetometer placed on the transversing table. This allowed the measurement of displacements in the horizontal direction accurate to 0.1 mm. The thermocouples were traversed at reduced revolutions. The cold junction of the thermocouple was located on the temperature-controlled surface of the rotating table, and the temperature was calculated from the temperature of the surface which modelled the growing face of the crystal.

The block diagram of synchronous measurements of the instantaneous e.m.f.s of the thermocouples is given in Fig. 5(b). The constant e.m.f. component of thermocouples 1 and 2 was compensated and measured by small-size potentiometers 3 and 4 which had been calibrated with the aid of a P-3003 comparator (5) accurate to 0.5 μV. The non-compensated e.m.f. component (with the comparator switched off) was amplified by a constant current amplifying coefficient. To attenuate the interference, the signal from the constant current amplifier was passed through a low-pass filter with a cut-off frequency of 1.5 Hz. The constant current amplifiers had a small noise ($\simeq 1$ μV) and zero drift of 1 μV h^{-1}. The analogue signals were recorded synchronously by a two-channel recorder H 3021-2.

Investigations were carried out when the modulated rotation of the bulb followed the trapezoidal law and had the parameters depicted in Fig. 7(a), with vertical orientation of the axis of rotation. The system used to measure the rotational speed made it possible to fix the change in time of the number of rotations by a self-recording potentiometer H 3012.

ISOTHERMAL CONDITIONS

The working fluid used was 96% ethyl alcohol. Flow visualization was accomplished with the aid of aluminum particles. The flow patterns were fixed by a movie camera 'Pentaflex-16' at a frame speed of 24 frames s^{-1}. As the film was taken, all the devices operated synchronously. The filming revealed the character of liquid flow in the bulb and at the growing face of the crystal and also gave the axial velocity of the ascending and descending flows. The motion pictures show that with modulated rotation under isothermal conditions periodic flows appear in the neighbourhood of the lower plane and the face of the cylinder (crystallization front): (a) when the number of revolutions decreases, there appears a vortex flow which is directed along the radius to the centre and axially upwards (Fig. 6(a)); (b) when the number of revolutions increases, there originates a flow near the crystallization front surface along the radius to the cylinder generatrix (Fig. 6(b)). The physical nature of these flows is as follows: when the number of revolutions of the bulb decreases, the liquid core has higher angular speed than the substrate and flows originate which are analogous to those induced near a fixed disk in a liquid rotating at a constant angular speed; due to retardation the decelerated liquid particles near the wall have a smaller centrifugal force and they move radially to the bulb axis; the total amount of liquid flowing toward the axis of rotation through the cylinder surface of radius r is equal to [18]

$$Q_1 = -1.38\pi r^2 \sqrt{(\bar{\omega}_1 \nu)} \qquad (23)$$

where $\bar{\omega}_1$ is the mean angular speed in the core in the period of retarded rotation.

As the number of rotations increases, the angular speed of the substrate becomes higher than that of the liquid in the core, and near the growing face of the crystal there appears a flow which is analogous to that about a disk rotating in a quiescent liquid: the liquid entrained into rotation in a thin boundary layer near the surface is rejected outwards by centrifugal forces;

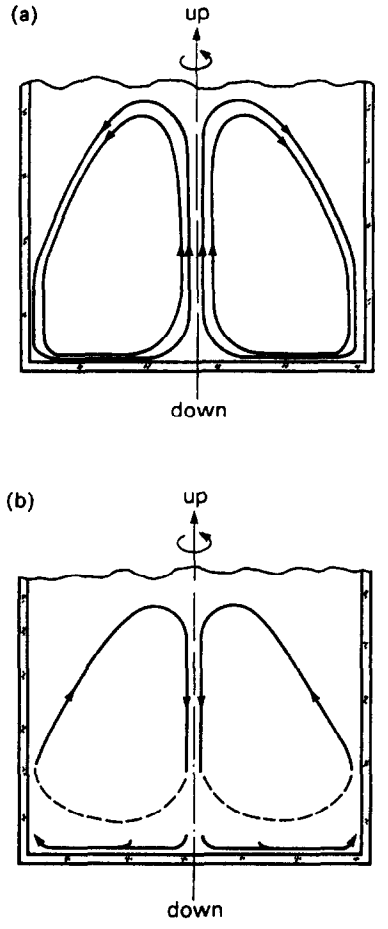

FIG. 6. (a) Direction of liquid stream lines in the bulb near the temperature-controlled substrate for decelerated rotation of the bulb. (b) Direction of liquid stream lines in the bulb near the temperature-controlled substrate for accelerated rotation of the bulb.

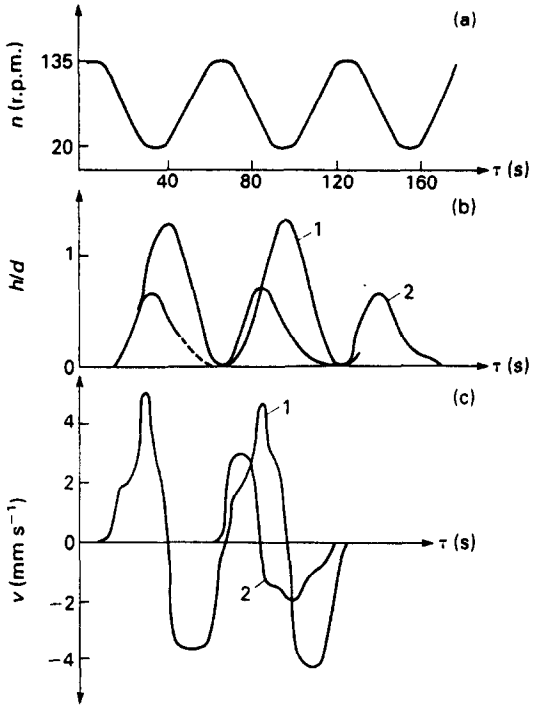

FIG. 7. (a) The law of modulated rotation. 1, Isothermal conditions. 2, Non-isothermal conditions. (b) Variation of the vortex height along the bulb axis ($H = 55$ mm). 1, Isothermal conditions. 2, Non-isothermal conditions. (c) Rate of change in the vortex height ($H = 55$ mm). 1, Isothermal conditions 2, Non-isothermal conditions.

the discharge rate of this liquid is given by [18]

$$Q_2 = 0.886\pi r^2\sqrt{(\bar{\omega}_2 \nu)} = 0.886\pi r^3 \bar{\omega}_2 \, Re^{-1/2} \quad (24)$$

where $\bar{\omega}_2$ is the mean angular speed of liquid rotation. At $\bar{\omega}_2 = \bar{\omega}_1$ the mean velocity $\bar{v}_1$ of the ascending flow is greater than that of the descending flow (v_2): $v_1/v_2 = 1.56$.

Figure 7(b) (curve 1) presents the change in the vortex height (h/d) with time and the rate of change in the vortex height, which also characterizes the speed of the rise and fall of the liquid in the vicinity of the axis for $H = 55$ mm. In Fig. 7(c) (curve 1) a change in the axial flow velocity (v) in the vicinity of the bulb axis is presented as a function of rotation modulation (Fig. 7(a)) under isothermal conditions. A periodic change of character in the axial velocity is observed and, consequently, in the radial velocity near the crystallization front. The ratio of the maximum velocities of the ascending ($v_{1,\max}$) and descending ($v_{2,\max}$) flows in the vicinity of the bulb axis ($v_{1,\max}/v_{2,\max} \simeq 1.4$) is close to that predicted theoretically, without regard for the end face effects on the edge of the disk.

FLOW STRUCTURE UNDER THE CONDITIONS OF STABLE STRATIFICATION

The temperature gradient along the bulb height was created by energizing the upper annular heater; the bottom of the bulb was temperature-controlled ($T_c = 24.5$°C). In the absence of rotation the time for operating regime establishment was equal to about 3 h. The temperature in the bulb core behaved exponentially, following from solution (2). This indicates that heat is removed through the side surfaces of the bulb. The heat removal through the lower end face is significant at high liquid heights.

In the case of modulated variation of the number of rotations a stable periodic flow originates after the second period of modulation; the amplitudes of periodic temperature fluctuations become constant after 15 periods of modulation. Under conditions of stable stratification the character of flow is somewhat different: the greatest dimension of the vortex decreases (Fig. 7(b), curve 2) as compared with the conditions of neutral stratification (Fig. 7(b), curve 1) and, because of the radial temperature gradient produced by the axial motion of the vortex is unstable and is 'blurred' on flow inversion.

Due to stable stratification near the bottom of the bulb, the velocities of the ascending and descending flows are smaller than those in the absence of a temperature gradient (Fig. 7(c)).

Measurements of the actual temperatures and their correlations were made along the radius at different fixed heights with the aid of the Γ-shaped thermocouple. The axial thermocouple probe was fixed in one position during the entire experiment.

Figures 8–11 present instantaneous temperatures for different distances (r) from the rotation axis and at a fixed vertical coordinate (H–y) for the heights of the liquid layer: $H = 64$, 47.2, 22.2 and 11.6 mm. Figures 12–15 show the temperature history at a fixed radius for different 'H–y' for the ethyl alcohol layer of heights $H = 64$, 47.2, 22.2 and 11.6 mm. In Figs. 8–15 the origin of time calculation ($\tau = 0$) corresponds to the start of the period of modulation at the point of the approach of $\omega = \omega_{max}$ shown in Figs. 10, 11, 14 and 15. It is seen from these plots that the influence of the wall flows at the end face caused by periodic variation of centrifugal forces is manifested along the entire height of the bulb. There is a close correlation

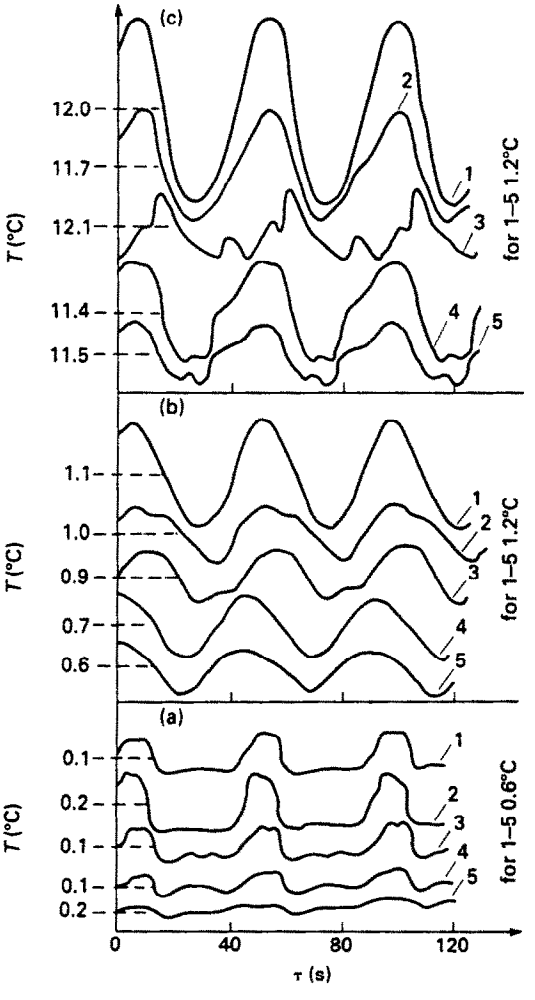

FIG. 8. Instantaneous values of temperature in the layer with $H = 64$ mm. (a) H–$y = 3.31$ mm: $r = 1.5$ mm (1), 2.5 mm (2), 5 mm (3), 8.1 mm (4) and 13.3 mm (5). (b) H–$y = 21.97$ mm: $r = 3.6$ mm (1), 5.7 mm (2), 8 mm (3), 11.6 mm (4) and 13.1 mm (5). (c) H–$y = 48.29$ mm: $r = 1.7$ mm (1), 3 mm (2), 8 mm (3), 11.3 mm (4) and 13.4 mm (5).

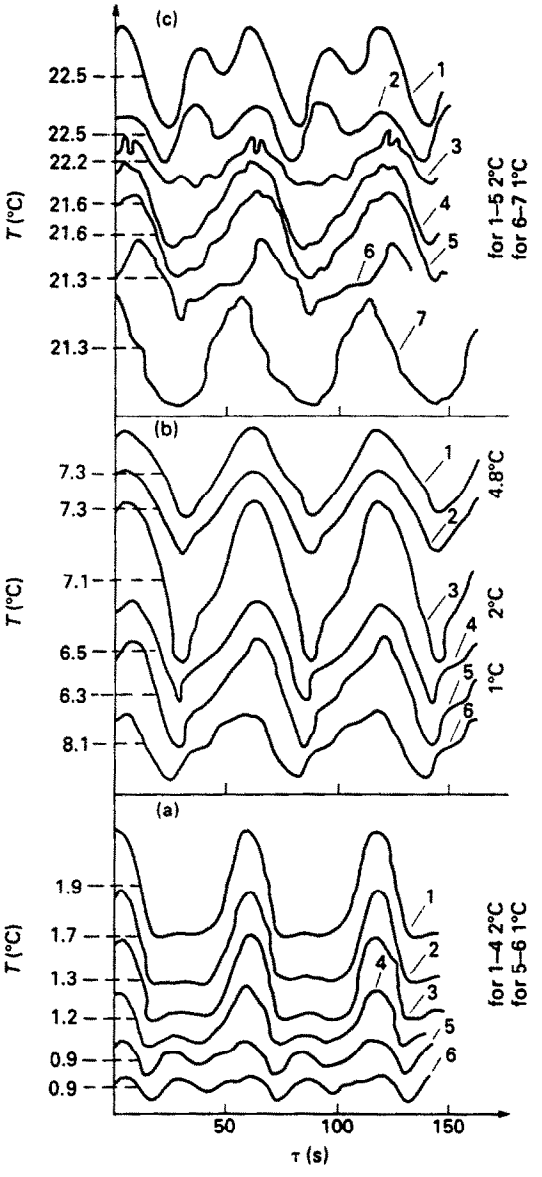

FIG. 9. Instantaneous values of temperature in the layer with $H = 47.2$ mm. (a) H–$y = 1.31$ mm: $r = 0.3$ mm (1), 3.15 mm (2), 6 mm (3), 8.1 mm (4), 11.6 mm (5) and 12.8 mm (6). (b) H–$y = 14.5$ mm: $r = 2.7$ mm (1), 6 mm (2), 7.7 mm (3), 10.3 mm (4), 12 mm (5) and 13.4 mm (6). (c) H–$y = 27.15$ mm: $r = 1.5$ mm (1), 3.6 mm (2), 7.5 mm (3), 8.8 mm (4), 9.1 mm (5), 11.4 mm (6) and 13 mm (7).

between the temperatures along the height and along the radius of the cylindrical bulb. In Fig. 16 instantaneous temperatures at the bottom (crystallization front) near the rotation axis are presented for different heights of the liquid layer ($H = 64$, 47.2, 22.2 and 11.6 mm). As the height of the liquid layer (working zone of the melt) decreases by a factor of six, the amplitude of temperature fluctuations increases 20 times (the drop between the temperatures of the lower end face and of liquid near the upper heater was constant). The actual temperatures were used to determine the mean temperatures with respect to time; the

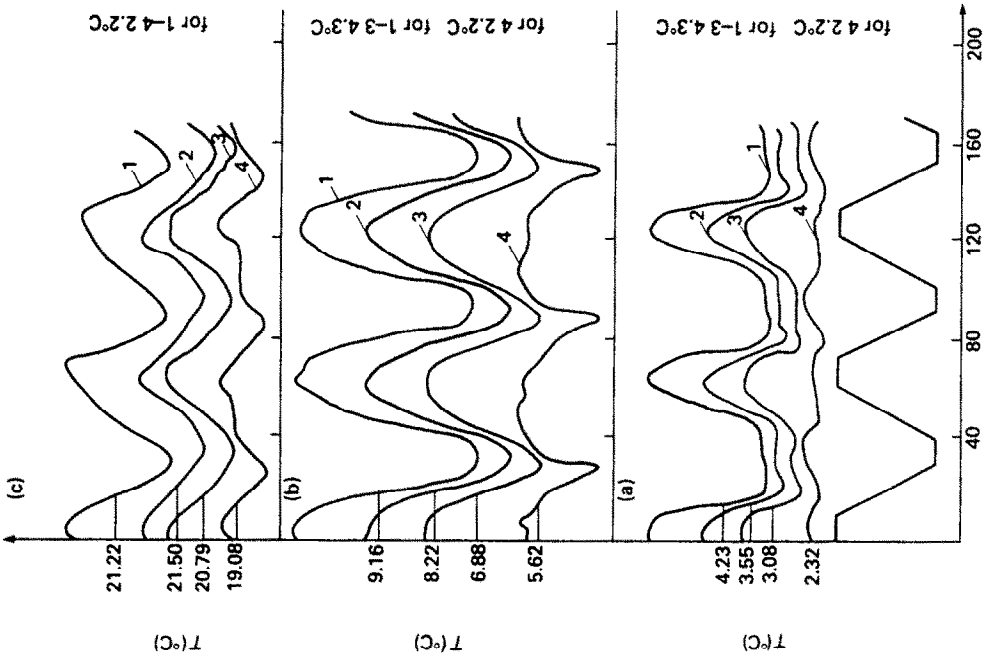

FIG. 10. Instantaneous values of temperature in a layer with $H = 22.2$ mm. (a) H, $r = 1.99$ mm: $r = 2.2$ mm (1), 6.6 mm (2), 8.7 mm (3) and 14.4 mm (4). (b) H, $r = 7.37$ mm: $r = 2.4$ mm (1), 6.4 mm (2), 9.3 mm (3) and 13 mm (4). (c) H, $r = 14.68$ mm: $r = 2.6$ mm (1), 6.2 mm (2), 8.1 mm (3) and 14.3 mm (4).

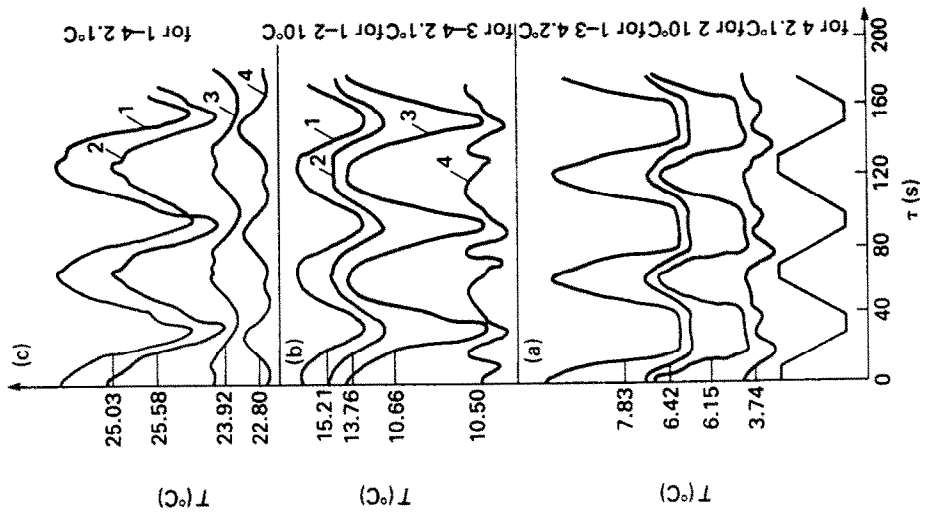

FIG. 11. Instantaneous values of temperature in a layer with $H = 11.6$ mm. (a) H, $r = 1.98$ mm: $r = 2.4$ mm (1), 5.6 mm (2), 7 mm (3) and 12.8 mm (4). (b) H, $r = 5.73$ mm: $r = 2.3$ mm (1), 6.5 mm (2), 9.9 mm (3) and 13.1 mm (4). (c) H, $r = 9.39$ mm: $r = 2.8$ mm (1), 5 mm (2), 9.8 mm (3) and 12.6 mm (4).

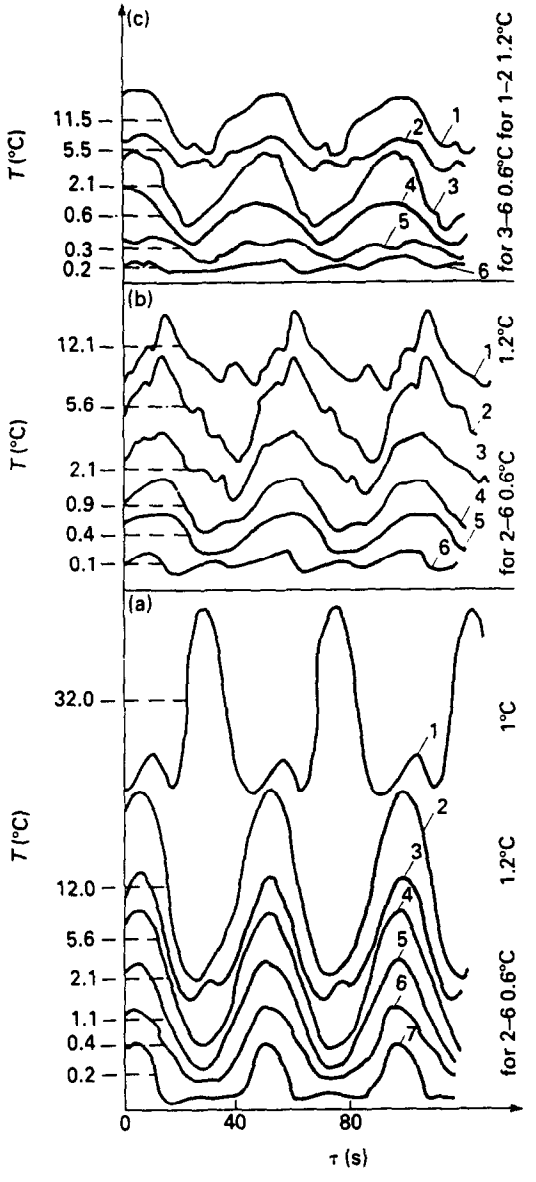

FIG. 12. Instantaneous values of temperature in a layer with $H = 64$ mm for $r = 2.7$ mm (a), 7.7 mm (b) and 13.4 mm (c) at $H-y = 48.29$ mm (1), 37.56 mm (2), 29.25 mm (3), 21.97 mm (4), 13.04 mm (5), 3.18 mm (6a,c), 3.33 mm (6b) and 60.26 mm (7).

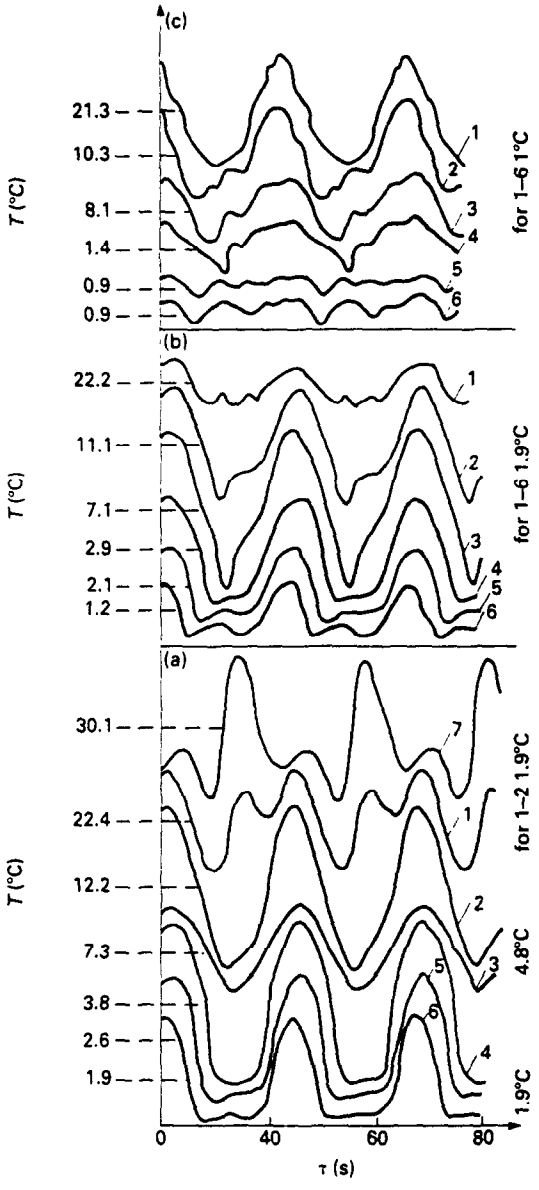

FIG. 13. Instantaneous values of temperature in a layer with $H = 47.2$ mm for $r = 1.7$ mm (a), 7.8 mm (b) and 13.4 mm (c) at $H-y = 27.15$ mm (1), 19.6 mm (2), 14.5 mm (3), 8.1 mm (4), 3.79 mm (5), 1.32 mm (6a), 1.35 mm (6b,c) and 30.75 mm (7).

mean temperatures for different radii being known, the average values at fixed distances from the lower end face could be determined.

In Fig. 17 the changes in the mean temperature in the flow core are presented for different distances from the upper heater (y) in the absence and presence of modulated rotation at $H = 55$ mm and modulation period $\tau = 60$ s. Just as in the case of the absence of rotation, the exponential law of temperature variation (2) is observed. The constant value of temperature for $y < 10$ mm is due to boiling on the heater. Because of the penetrating effect of liquid agitation caused by boiling, the constant temperature is also observed below the heater.

Modulated rotation induces only an insignificant increase of mean temperatures; the laws governing the change in the mean temperature, along the height of the flow core, both with and without modulated rotation, are dictated by heat removal along the generatrices of the bulb surfaces. Periodic variations of temperature throughout the entire volume of the bulb result from periodic variations in the speed of bulb rotation with the modulation period $\tau = 60$ s.

Figure 18 presents temperatures along the layer height for $H = 47.2$ and 64 mm. It is seen from Figs. 17 and 18 that, depending on the height of the layer and temperature at $y = 0$, the character of temperature variation near the growing face of the crystal

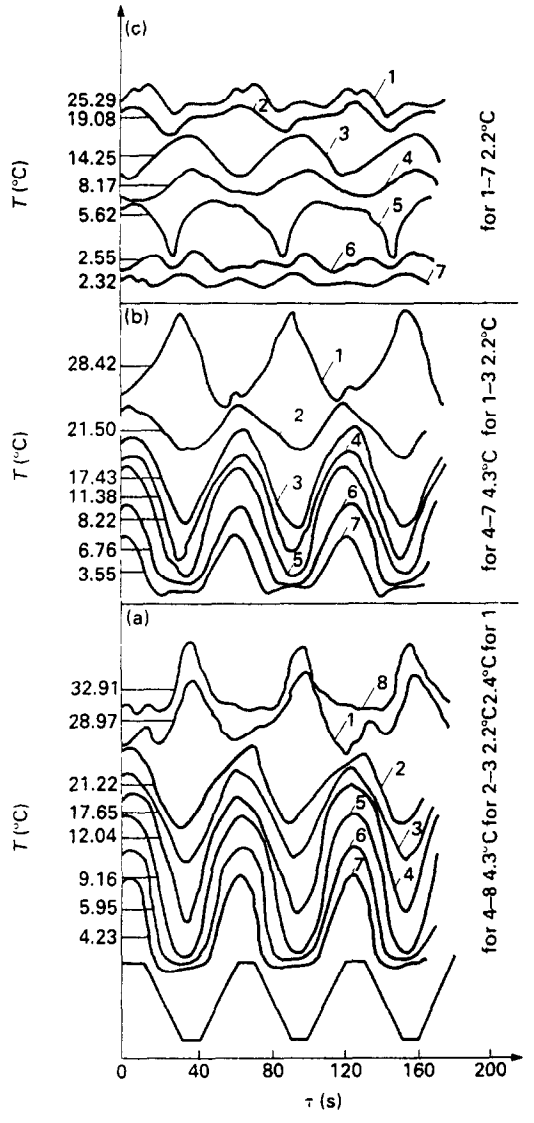

FIG. 14. Instantaneous temperature values in a layer with $H = 22.2$ mm for $r = 2.2$ mm (a), 6.6 mm (b) and 14.2 mm (c) at $H-y = 17.49$ mm (1), 14.68 mm (2), 12.63 mm (3), 9.76 mm (4), 7.37 mm (5), 4.17 mm (6), 1.99 mm (7) and 18.46 mm (8).

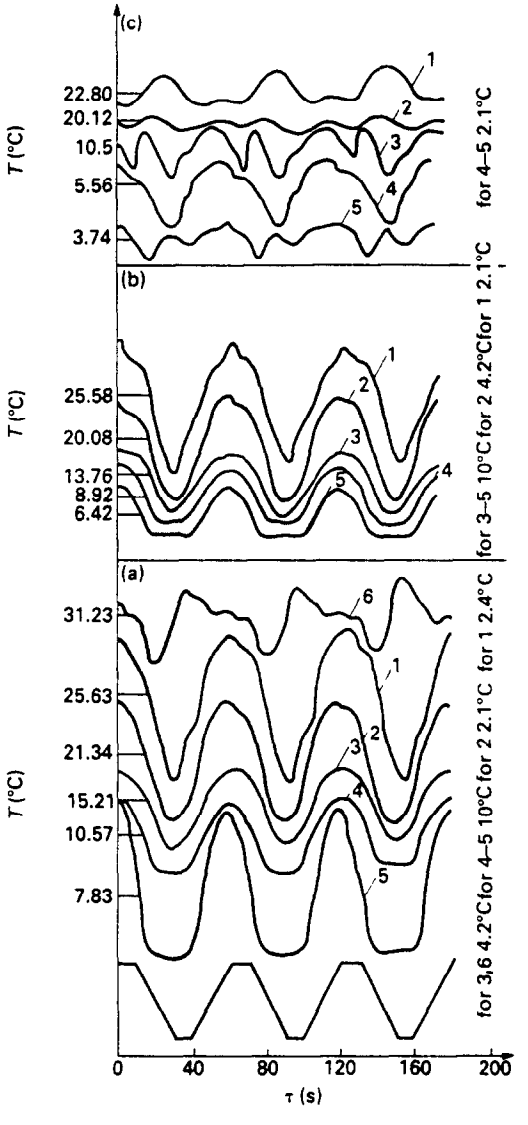

FIG. 15. Instantaneous values of temperature in a layer at $H = 11.6$ mm for $r = 2.5$ mm (a), 5.7 mm (b) and 12.8 mm (c) at $H-y = 9.39$ mm (1), 7.54 mm (2), 5.73 mm (3), 3.5 mm (4), 1.98 mm (5) and 10.35 mm (6).

is different. For a fixed value of T_{max} there is a height h_0 at which ($y = h_0$) $\partial T/\partial y \to 0$ near the bottom of the bulb. When $h > h_0$, the periodic temperature fluctuations at the substrate are insignificant in the case of modulated rotation of the bulb because in the neighbourhood of the bulb bottom $\partial T/\partial y \to 0$; as the height of the layer increases, the amplitude of temperature fluctuation at the bottom of the bulb ($y = H$) tends to zero. When $h < h_0$, the deviation of temperature from the exponent, equation (2), near the substrate of the bulb and increase in the temperature gradient near the bottom of the bulb are observed and, consequently, an increase in the amplitude of temperature fluctuations near the growing face of the crystal (see Figs. 17 and 18). Thus, by changing the position of a heat exchanger along the height of the bulb, it is possible to regulate the amplitude of temperature fluctuation at its bottom. By varying the law of modulation of the number of rotations it is possible to find the optimum period of temperature fluctuation near the growing face of the crystal. The amplitude of temperature fluctuation near the bottom of the bulb can also be regulated by the maximum and minimum angular rotational speeds of the bulb and also by its radius. By varying the above parameters it is possible to find the optimum temperature conditions for growing monocrystals of specific substances.

For all the heights of the layer investigated (from 11.6 to 64 mm) (see Figs. 17–19) there is a region where the change in the mean temperature over the

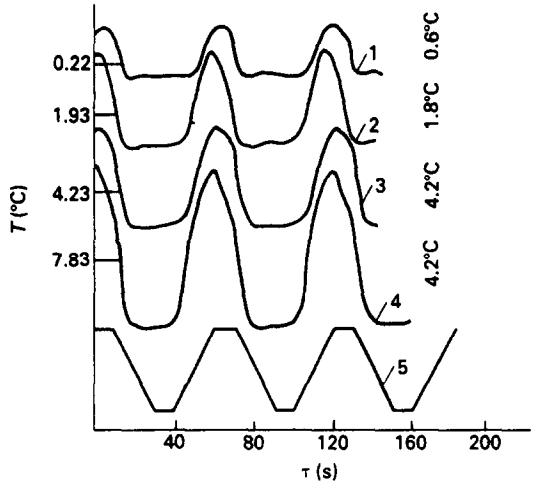

FIG. 16. Instantaneous values of temperature in a layer. 1, $H = 64$ mm; $H-y = 3.18$ mm, $r = 2.5$ mm. 2, $H = 47.2$ mm; $H-y = 1.32$ mm, $r = 0.3$ mm. 3, $H = 22.2$ mm, $H-y = 1.99$ mm, $r = 2.2$ mm. 4, $H = 11.6$ mm, $H-y = 1.99$ mm, $r = 2.4$ mm.

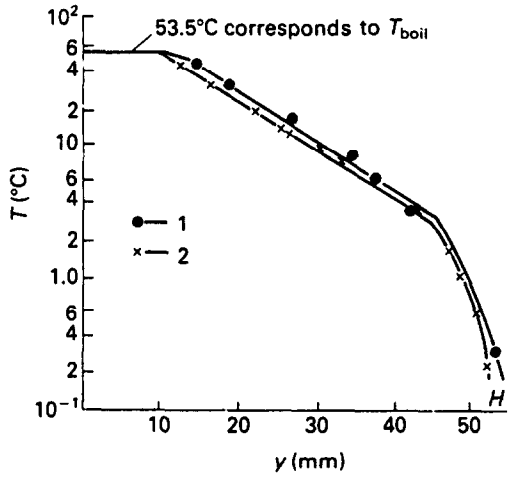

FIG. 17. Distribution of averaged temperature over the layer height ($H = 55$ mm). 1, Time-averaged temperatures at the section with $y = \text{const}$. (modulated rotation). 2, Averaged temperature at $y = \text{const}$.

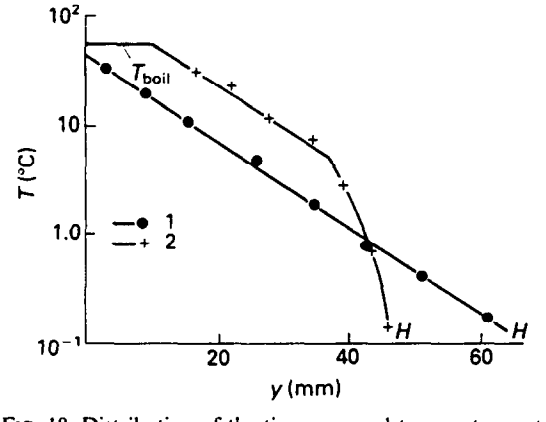

FIG. 18. Distribution of the time-averaged temperatures at the section with $y = \text{const}$. (modulated rotation). 1, $H = 64$ mm. 2, $H = 47.2$ mm.

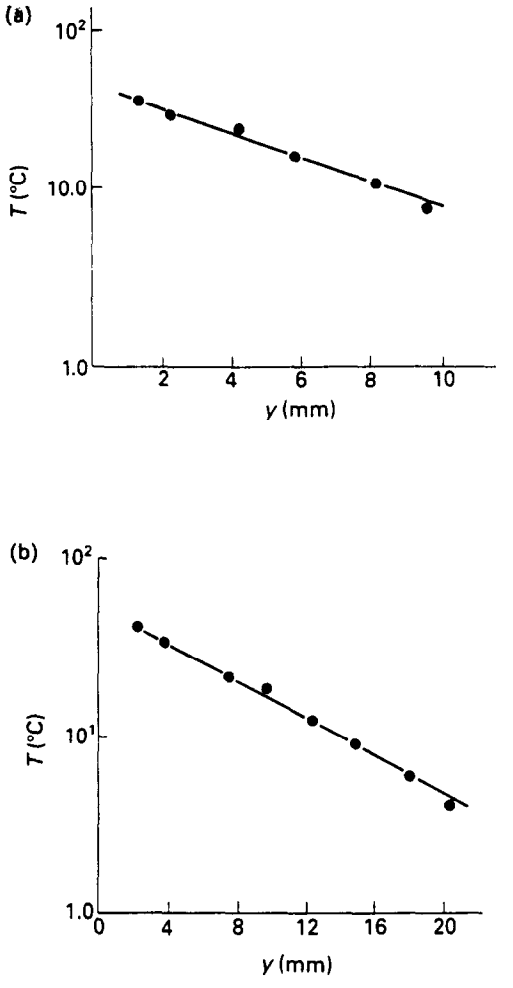

FIG. 19. (a) Distribution of the time-averaged temperatures at the section with $y = \text{const}$. (modulated rotation), $H = 11.6$ mm. (b) Distribution of time-averaged temperatures at the section with $y = \text{const}$. (modulated rotation), $H = 22.2$ mm.

height follows law (2). This indicates that in the case of a layer of small height (Fig. 19) heat is removed through the side generatrices of the cylinder.

The amplitude of temperature fluctuations (T_{max}, T_{min}) and mean temperature $\bar{T}$ at the fixed values of r for different distances from the bulb bottom are presented in Figs. 20–23. The amplitude of temperature fluctuations increases with distance from the bulb bottom, and at $H = 47.2$ mm the greatest $T_{max} - T_{min}$ value is observed at the height $(H-y)/r_0 = 1$ (Fig. 21), which is commensurable with the size of the vortex in the period of its developed flow.

When $H = 22.2$ mm (Fig. 22), the greatest $T_{max} - T_{min}$ values are observed at the height $(H-y)/r_0 = 0.5$, and for $H = 11.6$ mm (Fig. 23) at the height $(H-y)/r_0 = 0.4$ ($r = 2.5$–5.7 mm).

The maximum ascending and descending axial velocities can be assessed by assuming that temperature fluctuations due to heat conduction are much smaller than those due to convection. In this case, for fixed

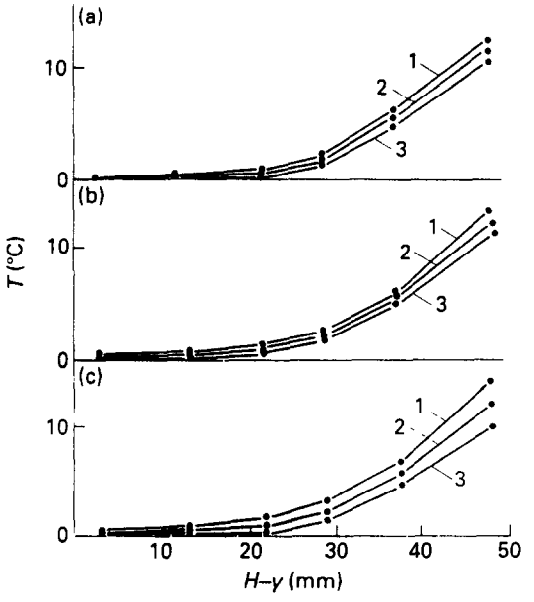

FIG. 20. Distribution of the maximum (1), mean (2) and minimum (3) temperatures over the layer height at $H = 64$ mm. (a) $r = 2.5$ mm; (b) $r = 7.5$ mm; (c) $r = 13$ mm.

values of r and y, the axial velocity can be estimated from the relation

$$v_{max} = \left(\frac{\partial T}{\partial \tau}\right)_{max} \left(\frac{\partial \bar{T}}{\partial y}\right)_{y}^{-1} \qquad (25)$$

where $\bar{T}$ is the mean temperature over the layer height and τ is the time. The value of v_{max} can be calculated approximately from the relation $v_{max} = \Delta y/\Delta\tau$, where Δy is determined for fixed y from the function $\bar{T}(y)$ (Figs. 20–23) and from the amplitude of temperature fluctuations; $\Delta\tau$ is found from the analogue representation of $T(\tau)$ corresponding to r and y (Figs. 8–15) and is the time for which the temperature varies from T_{max} to T_{min} at $(\partial T/\partial\tau)_{max}$ in the region of an increasing and decreasing temperature.

Figure 24 presents velocity variations of the descending and ascending flows for fixed τ (=2.5) at the heights of working liquid layer $H = 64$ and 47.2 mm. The greatest absolute velocities are observed at $H-y/r_0 = 0.25$. Figure 25 depicts variations in the velocities of the descending and ascending flows for fixed r (=2.5 mm) at the heights of the working liquid layer $H = 47.2$, 22.2 and 11.6 mm. As the height of the liquid layer varies from 47.2 to 22.2 and 11.6 mm, the maximum velocity of the ascending flow decreases from 2.5 to 0.5 and 0.33 mm s^{-1}, respectively; on the other hand, the maximum velocity of the descending flow decreases from 1.5 to 0.45 and 0.29 mm s^{-1}, respectively (Fig. 25); as the height of the layer decreases four times, the maximum velocity of the flows falls by about a factor of 8. In the first place, this is attributable to a decrease in the dynamic inertia of the layer because of liquid depletion and secondly to a decrease in the dynamic interaction between the

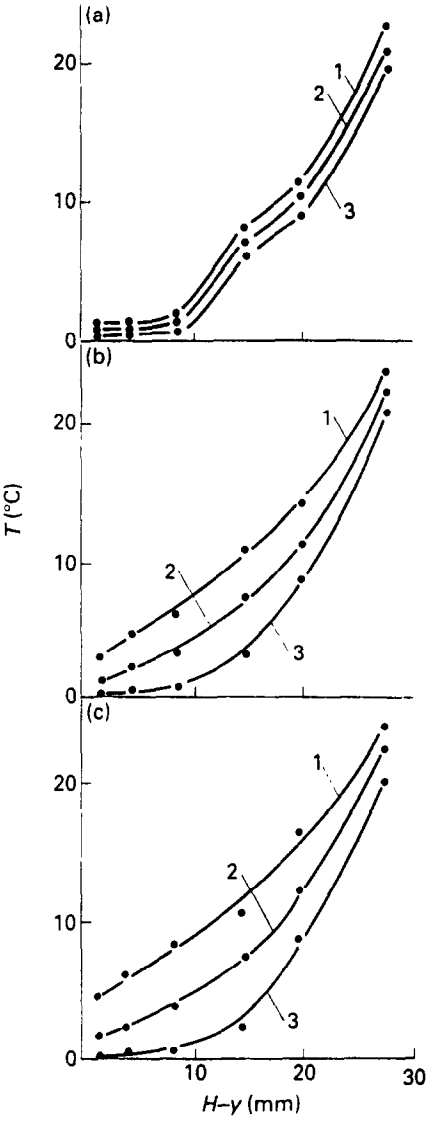

FIG. 21. Distribution of the maximum (1), mean (2) and minimum (3) temperature over the height of the layer at $H = 47.2$ mm. (a) $r = 2.5$ mm; (b) $r = 7.5$ mm; (c) $r = 13$ mm.

cylinder walls and the liquid, because the area of wetting of cylinder walls with the liquid is reduced with a decrease in the layer height. As the height of the liquid layer decreases, the axial temperature gradient near the lower end face of the cylinder (growing facet) increases, thus producing stable stratification and, consequently, the intensity of axial flows at the same values of n_{min} and n_{max} decreases.

Thus, with a decrease in the height of the working layer (which models the distance from the diaphragm of the growth furnace to crystallization front), the axial temperature gradient and the amplitude of temperature fluctuations at the bottom of the bulb increase and the amplitude of the axial velocity and its absolute values decrease.

The present authors used the trapezoidal law of

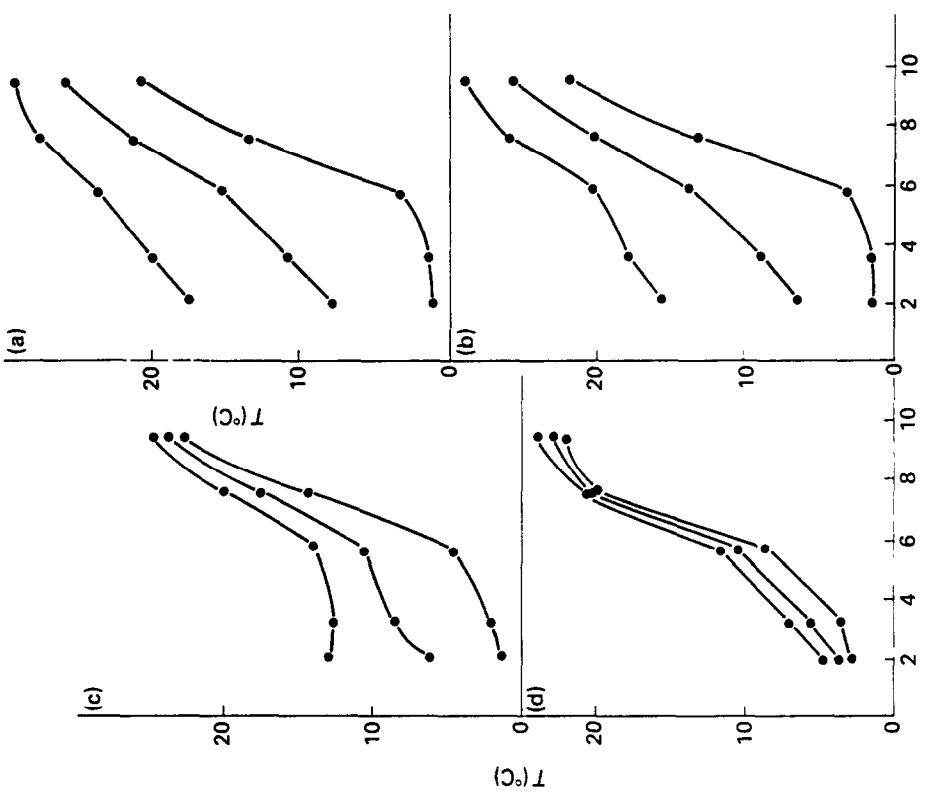

FIG. 23. Distribution of the maximum (1), mean (2) and minimum (3) temperatures over the layer height at $H = 11.6$ mm. (a) $r = 2.5$ mm; (b) $r = 5.7$ mm; (c) $r = 9$ mm; (d) $r = 12.8$ mm.

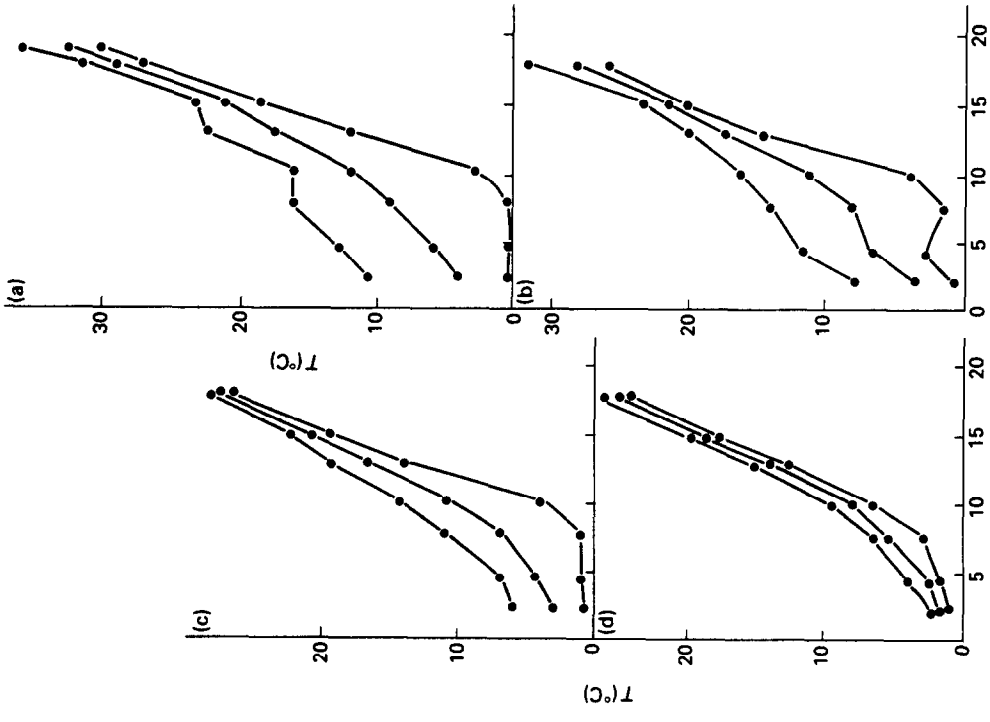

FIG. 22. Distribution of the maximum (1), mean (2) and minimum (3) temperatures over the layer height at $H = 22.2$ mm. (a) $r = 2.2$ mm; (b) $r = 6.6$ mm; (c) $r = 9.2$ mm; (d) $r = 14.2$ mm.

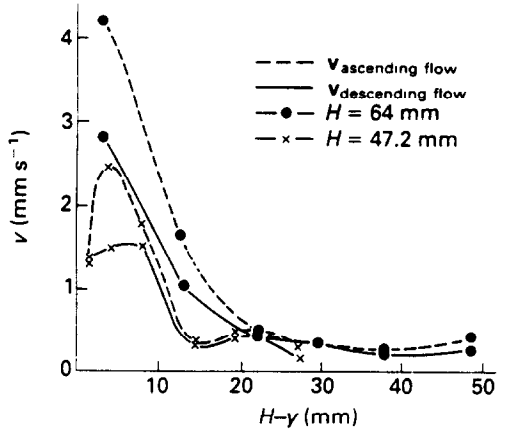

FIG. 24. Maximum velocities of the descending and ascending flows over the layer height at $r = 2.5$ mm. 1, $H = 64$ mm. 2, $H = 47.2$ mm.

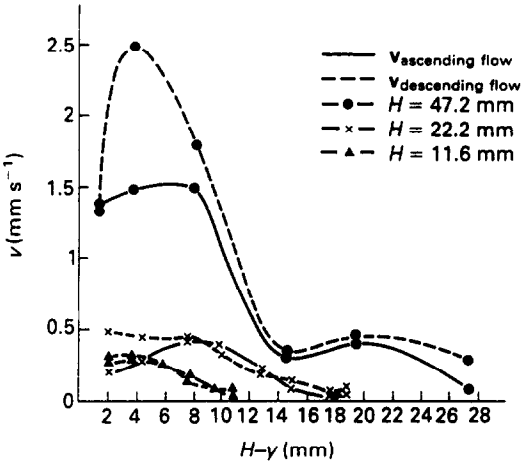

FIG. 25. Maximum velocities of the descending and ascending flows over the layer height at $r = 2.5$ mm. 1, $H = 47.2$ mm. 2, $H = 22.2$ mm. 3, $H = 11.6$ mm.

variation in the rotational speed of the cylindrical bulb (Fig. 7(a)). The characteristic times for this law are: the time (τ_1) during which the rotational speed increases linearly with time from the minimum to maximum value; the time (τ_2) during which a constant value of the maximum speed of rotation is observed; the time (τ_3) for which the rotation slows down to the minimum speed; the time (τ_4) in the course of which the rotational speed is constant and equal to the minimum. Depending on these time intervals, the intensity of vortex flows may be different. For example, at the greatest value of τ_2 the conditions are possible under which the angular speed of rotation of the liquid and the bulb will be the same and the vortex flow near the bottom of the cylinder will damp. The same phenomenon may also occur on an increase of τ_4. If the times τ_2 and τ_4 are taken to be small, the optimal (for these conditions) intensities of vortex flow near the cylinder end face may not be attained. At great τ_1 the difference between the angular speeds of rotation of the bulb and liquid can be small and, consequently, there will be a low intensity of wall flows near the cylinder end face. On the other hand, an increase in the speed of rotation or its stepwise decrease ($\tau_1 \to 0$; $\tau_3 \to 0$) may lead to perturbations along the cylinder generatrices and at the lower end face (for example, a sharp decrease in the speed of rotation may cause the appearance of Taylor vortices near the cylinder generatrices).

To determine the optimal parameters of modulation of the rotational speed, investigations of the system inertia were carried out and, consequently, of the decay of vortex flows after the attainment of the maximum and minimum speeds. In this case it is possible to estimate the level of τ_2 and τ_4 at the given n_{min} and n_{max}, the cylinder diameter, height of the liquid layer and temperature drop between the cylinder end face and the upper heated liquid layer.

The experiments were carried out as follows. The regime of modulated rotation was set when periodic changes of temperature attained constant amplitude values; as the n_{max} value was reached, it was stabilized ($n_{max} = \text{const.}$) as long as was necessary ($\tau_2 \to \infty$) and the change of temperature with time was fixed. The time (τ_{max}) during which the temperature attained its constant value was found from the plots (Fig. 26) as the instant at which the temperature deviation from the exponential relation was fixed. The same technique was used to determine the time τ_{max} for velocity

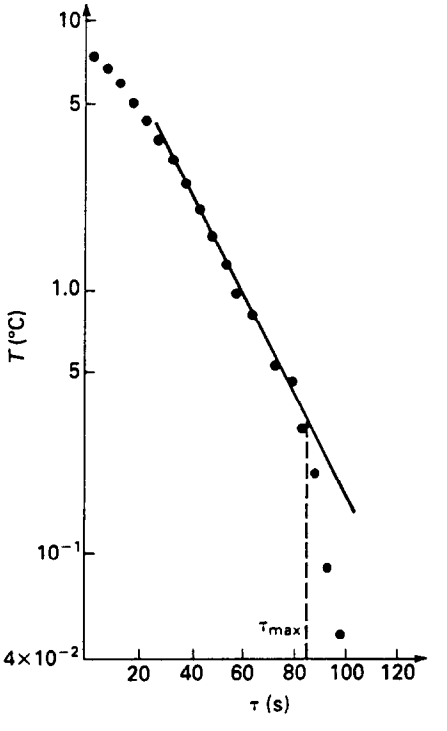

FIG. 26. Dependence of the temperature (T) on time (τ) at the stabilized speed of container rotation ($\omega_{max} = \text{const}$, $H = 22.4$; $H-y = 6.09$ mm).

stabilization to its minimum value. The value of τ_{max} was determined at $r = 0$ at the heights of the ethyl alcohol layer $H = 54.6$ and 22.4 mm, $n_{max} = 135$ r.p.m., $n_{min} = 20$ r.p.m. (Figs. 27(a) and (b)). As follows from Fig. 27(a), with n_{min} = const. and decreasing height of the layer, τ_{max} increases and for $H = 54.6$ and 22.4 mm the values of τ_{max} were 110 and 160 s, respectively (H–$y = 8$ and 6 mm). The mean values of $\bar{\tau}_{max}$ were 50 and 100 s, respectively, for $H = 54.6$ and 22.4 mm. At n_{max} = const. the mean values $\bar{\tau}_{max}$ varied little for these heights and $\bar{\tau}_{max} \approx 75$ s.

The quantity τ_{max} characterizes the magnitude of the thermal inertia of the layer, which also depends on the hydrodynamic inertia. In the experiments considered it was impossible to determine the contribution of each of them to τ_{max}.

For finding the optimal values of the 'time shelves' of τ_2 and τ_4 (from the viewpoint of mixing), it is necessary to know the hydrodynamic inertia of the process. With this method of determination of τ_{max} it is nevertheless possible to estimate the greatest values of the quantities τ_2 and τ_4.

The method of modulated rotation of the crucible in the process of growing single crystals from the melt by the Stockbarger method was applied for the first time by the present authors [14–16] to obtain single crystals of proustite of large diameter and high optical quality. The speed of rotation of the crucible in the process of growth varied by the trapezoidal law (analogous to rotational speed variation used in model experiments). The experiments on growing proustite monocrystals confirmed the great possibilities of the technique for growing large optical crystals. As shown earlier [20], the proustite monocrystals of high optical quality with diameters above 24 mm can be grown only at a certain intensity of melt mixing (the relative Taylor number of $Ta_{rel} = Ta/Ta_0 > 0.42$): as Ta_{rel} increases, the optical quality of the monocrystal is improved. The optical quality of monocrystals was estimated by the value of the absorption coefficient in the visible and IR parts of the spectrum and also by optical revolutions. A direct relationship has been found between the increase in the intensity of mixing of proustite melt and a decrease in the absorption coefficients of monocrystals. Figure 28 presents the dependence of the absorption coefficients for an ordinary beam (K_0) (at a wavelength of 0.78 μm), which is one of the criteria of optical quality of the crystal relative Taylor number which characterizes the intensity of melt mixing. Solid lines connect the points that have a strictly fixed composition. As the relative Taylor number increases, the absorption coefficients decrease, i.e. the optical quality of monocrystals improves. Consequently, for monocrystals of different substances grown by the Stockbarger method with application of the ACR technique, it is possible, by using the results of model experiments, to determine the required (for a certain diameter of the container) regime of the speed of crucible rotation. It must be taken into account that the quantitative estimates and comparisons with the present experiment can be made only if the thermophysical characteristics of the melts

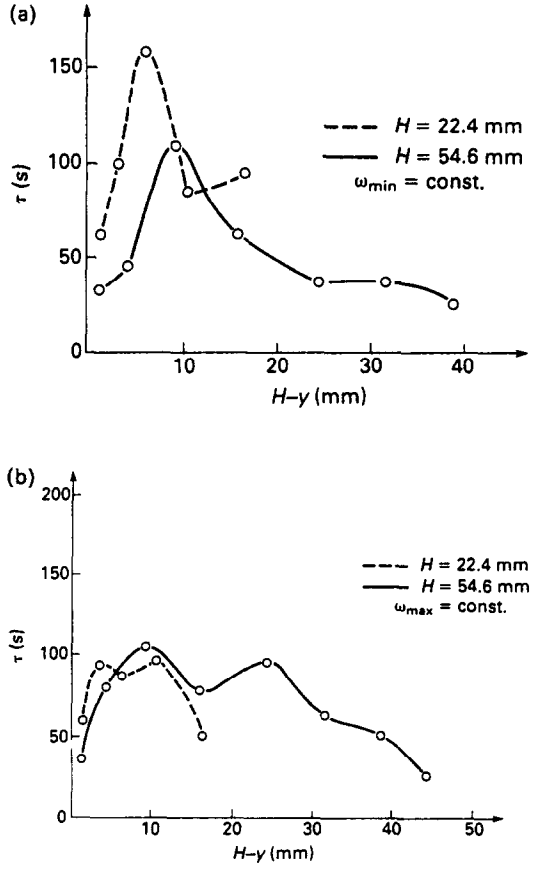

FIG. 27. (a) Dependence of the time temperature (τ_{max}) stabilization on the height of the melt (H–y) at ω_{min} = const. ($H = 54.6$ mm; $H = 22.4$ mm). (b) Dependence of the time temperature (τ_{max}) stabilization on the height of the melt (H–y) at ω_{max} = const. ($H = 54.6$ mm; $H = 22.4$ mm).

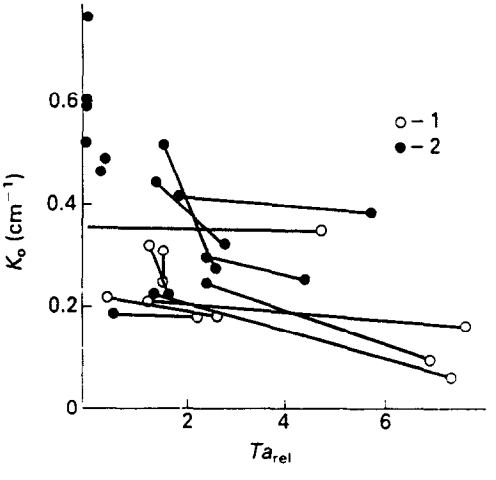

FIG. 28. Dependence of the absorption coefficients on the relative Taylor number ($\lambda = 780$ nm). 1. Monocrystals with the optical resolution (ϕ/ϕ_0) < 1.06. 2. Crystals with small-angle boundaries.

of the substances studied are known and the corresponding criteria of the process are considered.

CONCLUSIONS

In the case of periodic variation of centrifugal forces in a vertical cylinder, the axis of which coincides with the axis of its rotation, a periodic vortex flow originates near the lower rigid end face of the cylinder, the direction of which depends on whether the speed of cylinder rotation is accelerated or decelerated.

With heating from above and cooling near the lower end face (in the absence of rotation), a descending free convection boundary layer is formed along the cylinder generatrices; in the core of the cylindrical liquid layer the temperature varies exponentially along the height.

With mutual effect of the thermal gravitational and periodically varying centrifugal forces, the structure of liquid flow near the lower end face remains intact; the temperature gradient near the lower end face, while producing stable stratification of liquid, somewhat suppresses the vortex flow, thus decreasing the greatest size of the vortex, and induces an unstable flow in it due to the presence of the horizontal temperature gradient.

In the case of a periodic law of variation in the number of cylinder revolutions, the periodic variation of temperature takes place throughout the entire liquid layer. The averaged temperature in the flow core, except for the wall boundary layers, varies just as in the case without rotation, following the exponential law. This indicates that the time-averaged temperature field in the liquid is also formed under the influence of heat gravitational flows.

As the height of the layer decreases, the temperature amplitude increases and the velocity amplitude decreases due to the increase in the temperature gradient and decrease in the dynamic inertia of the layer.

The flows originating under the action of a periodically varying centrifugal force can be used as a means of controlling the mixing of a melt near the growing face of the crystal when growing monocrystals from melts in cylindrical bulbs by the Stockbarger method.

REFERENCES

1. A. N. Kirgintsev (Editor), *Controlled Crystallization in a Tubular Container*. Izd. Nauka, Novosibirsk (1978).
2. A. P. Kapustin, *The Effect of Ultrasound on the Kinetics of Crystallization*. Izd. AN SSSR, Moscow (1962).
3. Kh. S. Bagdasarov, *Application of Ultrasound in Industry*. Mashgiz, Moscow (1959).
4. H. J. Sheel and E. O. Shultz-Du Bois, Flux growth of large crystals by accelerated crucible-rotation technique, *J. Crystal Growth* **8**, 304–306 (1971).
5. E. O. Shultz-Du Bois, Accelerated crucible rotation: hydrodynamics and stirring effect, *J. Crystal Growth* **12**, 81–87 (1972).
6. W. H. Grodkiewicz, E. F. Deaborn and L. G. van Uitert, In *Crystal Growth* (Edited by H. S. Peiser). Pergamon Press, Oxford (1967).
7. H. J. Sheel, Accelerated crucible rotation: a novel stirring technique in high-temperature solution growth, *J. Crystal Growth* **13/14**, 560–565 (1972).
8. G. Wende and P. Görnert, Study of ACRT by the high-resolution induced striation method, *Phys. Stat. Sol. (a)* **41**, 263–270 (1977).
9. P. Görnert, S. Bormann and R. Hergt, Investigation of the growth mechanism in high-temperature solutions by induced striation method, *Phys. Stat. Sol. (a)* **35**, 583–590 (1976)
10. V. Sip and V. Vanicek, *Growth of Crystals*, Vol. 3. Consultants Bureau, New York (1962).
11. T. L. Chu, M. Gill and P. K. Smeltzer, Growth of boron monophosphide crystals with the accelerated container rotation technique, *J. Crystal Growth* **33**, 53–57 (1976).
12. W. Tolksdorf and F. Welz, The effect of local cooling and accelerated crucible rotation on quality of garnet crystals, *J. Crystal Growth* **13/14**, 556–570 (1972).
13. N. J. Bollen, M. J. Essen and W. N. Smit, A fast method of zone melting as an aid in analytical chemistry, *Anal. Chim. Acta* **38**, 279–284 (1967).
14. A. A. Godovikov, V. E. Distanov, S. I. Lobanov, S. P. Popov, V. K. Chimiryov, Yu. A. Chulshchanov and M. G. Chulshchanova, Conditions for growing proustite monocrystals of higher optical quality. In *The Synthesis and Growing of Optical Crystal and Jewelry Stones*, pp. 4–10. Novosibirsk (1981).
15. V. E. Distanov and B. G. Nenashev, Optimization of the conditions of growth of monocrystals with regard for the hydrodynamics of the melt, *Extended Abstracts of the 2nd All-Union Seminar on the Hydrodynamics and Heat-Mass Transfer in Weightlessness*, pp. 33–34. Perm (1981).
16. A. A. Godovikov, V. E. Distanov and B. G. Nenashev, The application of the forced stirring of the melt during the high optical quality single crystal growth by the Bridgman–Stockbarger method, *European Meeting on Crystal Growth '82* (23–27 August 1982, Prague, Czechoslovakia) *Materials for Optoelectronics, Posters*, pp. 305–306.
17. A. Horowitz, D. Gazit and J. Makovsky, Bridgman growth of Rb_2MnCl_4 via accelerated crucible rotation technique, *J. Crystal Growth* **61**, 322–328 (1983).
18. H. Schlichting, *Grenzschicht-Theorie*. Verlag G. Braun, Karlsruhe (1964).
19. V. D. Zimin, Yu. N. Lyakhov and M. P. Sorokin, Convection in a vertical cylinder heated from above. In *Hydrodynamics*, No. VI, pp. 73–84. Perm (1975).
20. V. E. Distanov, A. G. Kirdyashkin and B. G. Nenashev, Application of forced mixing for growing monocrystals by the Bridgman–Stockbarger method. In *Materials of the Genetic and Experimental Mineralogy. Growth of Crystals*, pp. 21–43. Izd. Nauka, Novosibirsk (1988).

HYDRODYNAMQIUE ET TRANSFERT THERMIQUE DANS UN CYLINDRE VERTICAL EXPOSE A DES FORCES CENTRIFUGES VARIABLES PERIODIQUEMENT (TECHNIQUE DE LA ROTATION ACCELEREE)

Résumé—On étudie les aspects thermiques et hydrodynamiques de l'écoulement liquide dans un cylindre vertical exposé à l'effet simultané de forces thermiques gravitationnelles et de forces centrifuges variant périodiquement. Ces dernières sont produites par une variation périodique de la vitesse de rotation du cylindre dont l'axe coïncide avec celui de la rotation. Un écoulement vortex apparait à la base du cylindre et sa direction dépend de la vitesse de rotation. On étudie l'hydrodynamique et le transfert thermique d'un liquide stratifié de façon stable et exposé aux forces centrifuges périodiquement variables. On montre qu'il y a des changements périodiques de température dans toute la couche liquide ; les valeurs des températures et des vitesses ainsi que leurs variations sont données pour différentes hauteurs de couche liquide. On analyse l'effet des forces variant périodiquement sur la qualité de la croissance d'un cristal. L'étude peut intéresser les thermiciens et les spécialistes de la croissance des monocristaux.

HYDRODYNAMIK UND WÄRMEÜBERGANG IN EINEM VERTIKALEN ZYLINDER UNTER DEM EINFLUSS PERIODISCH VARIIERTER ZENTRIFUGALKRÄFTE

Zusammenfassung—Die thermische und hydrodynamische Struktur einer Flüssigkeitsströmung in einem senkrechten Zylinder wird unter der Bedingung untersucht, daß gleichzeitig thermische Auftriebskräfte und periodisch variierende Zentrifugalkräfte wirksam sind. Letztere werden durch eine periodische Variation der Rotationsgeschwindigkeit des Zylinders um seine Achse hervorgerufen. Am Boden des Zylinders ergibt sich eine Wirbelströmung, deren Richtung von der Rotationsgeschwindigkeit abhängt. Die Flüssigkeit ist stabil über die Höhe geschichtet—für diesen Fall werden die Hydrodynamik und die Wärmeübertragung bei periodisch veränderlicher Zentrifugalkraft untersucht. Es ergeben sich periodische Temperaturschwankungen innerhalb der gesamten Flüssigkeit; die Temperaturen und Geschwindigkeiten und deren Veränderungen entlang der Höhe werden ermittelt. Darüberhinaus wird der Einfluß der periodische veränderlichen Kräfte auf das Wachstum eines Kristalls analysiert. Die vorliegende Arbeit kann für Thermophysiker und Spezialisten auf dem Gebiet des Wachstums von Einkristallen interessant sein.

ГИДРОДИНАМИКА И ТЕПЛООБМЕН ПРИ ПЕРИОДИЧЕСКОМ ИЗМЕНЕНИИ ЦЕНТРОБЕЖНЫХ СИЛ В ВЕРТИКАЛЬНОМ ЦИЛИНДРЕ (МЕТОД ACRT)

Аннотация—Представлены исследования тепловой и гидродинамической структуры течения жидкости в вертикальном цилиндре при совместном влиянии тепловых гравитационных и периодически изменяющихся дентробежных сил. Последние создавались периодическим изменением чисел оборотов вращения вертикального цилиндра, ось которого совпадает с осью вращения. Обнаружено вихревое течение у нижнего торца, направление в котором зависит от того, увеличиваются или уменьшаются числа оборотов вращения цилиндра. Представлены исследования гидродинамики и теплообмена устойчиво стратифицированной по высоте жидкости при периодическом изменении центробежных сил. Показано, что периодические изменения температуры наблюдаются по всему слою; найдены амплитудные значения температуры и скорости и изменения их для различных высот слоя жидкости. Анализируется влияние периодического изменения сил на качество растущего кристалла. Работа представляет интерес для теплофизиков и специалистов по выращиванию монокристаллов.